

Carbonized wood with ordered channels decorated by NiCo₂O₄ for lightweight and high-performance microwave absorber

Guangyu Qin

Harbin Institute of Technology

X.X. Huang (✉ swliza@hit.edu.cn)

Harbin Institute of Technology

Xu Yan

Beijing institute of radio measurement

Yunfei He

Harbin Institute of Technology

Yuhao Liu

Harbin Institute of Technology

Long Xia

Harbin Institute of Technology Weihai

Bo Zhong

Harbin Institute of Technology Weihai

Research Article

Keywords: Microwave absorption, Wood-derived carbon, ordered channels architecture, Lightweight, Finite Element Analysis

Posted Date: May 4th, 2021

DOI: <https://doi.org/10.21203/rs.3.rs-479425/v1>

License: © ⓘ This work is licensed under a Creative Commons Attribution 4.0 International License.

[Read Full License](#)

Version of Record: A version of this preprint was published at Journal of Advanced Ceramics on December 24th, 2021. See the published version at <https://doi.org/10.1007/s40145-021-0520-z>.

**Carbonized wood with ordered channels decorated by NiCo₂O₄ for lightweight
and high-performance microwave absorber**

Guangyu QIN ^a, Xiaoxiao HUANG ^{a,*}, Xu YAN ^b, Yunfei HE ^a, Yuhao LIU ^a,

Long XIA ^{c,*}, Bo ZHONG ^c

^a *School of Materials Science and Engineering, Harbin Institute of Technology,*

Harbin, 150001, P. R. China,

^b *Beijing Institute of Radio Measurement, Beijing, 100854, P. R. China.*

^c *School of Materials Science and Engineering, Harbin Institute of Technology at*

Weihai, Weihai, 264009, P. R. China.

***Corresponding Author**

E-mail: Xiaoxiao Huang, swliza@hit.edu.cn.

Long Xia, xialonghit@gmail.com.

Abstract

Wood-derived carbon has a 3D porous framework composed of through channels along the growth direction, which is a suitable matrix for preparing electromagnetic wave (EMW) absorbing materials with low-cost, light-weight, environmentally friendly and excellent MA performance. Herein, the carbonized wood decorated by short cone-like NiCo_2O_4 (CW@ NiCo_2O_4) with highly ordered straightway channels architecture were successfully manufactured through a facile calcination procedure. Finite Element Analysis (FEA) simulation is carried out to detect the interaction between the prepared material and EMW when the ordered channels are arranged in different directions. Simultaneously, the microwave absorption properties of all samples are investigated in terms of complex permittivity and permeability. The horizontal arrangement of the through channels of CW@ NiCo_2O_4 (H-CW@ NiCo_2O_4) exhibits a strong reflection loss value of -64.0 dB at 10.72 GHz with a thickness of 3.62 mm and a low filling ratio of 26wt% (with the density of $0.98\text{g}\cdot\text{cm}^{-3}$), and the effective absorption bandwidth (EAB) is 8.08 GHz (9.92-18.0 GHz) at the thickness of 3.2 mm. The extremely advantageous structure of H-CW@ NiCo_2O_4 is the key to achieving excellent MA property, which enables multiple EMW loss mechanisms to be effectively realized. What's more, the introduction of NiCo_2O_4 increases the values of ϵ' and ϵ'' , resulting in enhanced dielectric loss. This research provides a low-cost, sustainable and environmentally friendly strategy for using carbonized wood to fabricate microwave absorbers with strong attenuation capabilities and lightweight.

Keywords

Microwave absorption; Wood-derived carbon; ordered channels architecture; Lightweight; Finite Element Analysis

1. Introduction

Due to the serious problem of electromagnetic pollution and the urgent need of military anti-reconnaissance capabilities, a variety of electromagnetic wave (EMW) absorbing materials with excellent performance have been developed, which attenuate EMW by converting them into other forms of energy [1, 2]. Among various microwave absorbing materials, the carbonaceous materials have been paid high attention due to their chemical stability, low density and tunable electromagnetic parameters. In past reports, commonly used carbon materials for microwave absorption (MA), such as carbon fiber [3], carbon nanotube (CNT) [4, 5] and graphene [6], exhibited good MA performance. Carbon materials have greatly promoted the development of absorbing materials.

Simultaneously, the concept of sustainable development and environmental friendliness is also being valued more and more. Traditional carbon materials often rely on modern industrial techniques, which are complex and costly, and the by-products of the preparation process can damage the natural environment. Fortunately, the biomass-derived carbon overcome the shortcomings of man-made carbon materials with many characteristics such as light weight, large natural reserves and low cost. Nowadays, the natural wood-derived carbon materials with through channels parallel to the growth direction have been successfully applied in many fields, for example, energy storage materials, catalysts and sensors [7-9]. The three-dimensional (3D) skeleton composed of orderly-arrangement and through channels existing in wood-derived carbon can also be applied to MA materials, which not only is favor of microwave scattering and multi-reflections to prolong the propagation path of EMW [10] and forms an efficient conductive network to enhance the conductive loss [11], but also provides a load position for magnetic materials to improve impedance matching and cause magnetic loss [12]. Hence, this 3D porous structure can be used as an ideal carbon substrate for electromagnetic interference (EMI) shielding and MA materials.

Xi et al. reported that wood-based straightway channel structure, which was analogous to a waveguide, exhibited excellent MA performance with maximum reflection loss (RL) of -68.3 dB at 4.28 mm and effective absorption bandwidth (RL <

-10 dB) up to 7.63 GHz at 3.73 mm [13]. This unique structure has provided inspiration for the subsequent design of wood-derived carbon MA materials. Zheng et al. have successfully fabricated the wood-derived magnetic porous carbon composites with a highly ordered anisotropic porous architecture on the foundation of the 3D orderly-channel skeleton, this Ni/porous carbon composite exhibited an exceptional EMI shielding effectiveness of 50.8 dB at the whole X band (8.2-12.4 GHz) with the thickness of 2 mm [11].

In order to make full use of the 3D ordered porous framework derived from wood-derived carbon, our research introduces NiCo₂O₄ mixture on the wall of highly ordered straightway channels inherited from wood. The NiCo₂O₄, a spinel-structure bimetal oxide, owns high electrochemical activity, was mainly used in the electrochemistry field[14, 15]. Therefore, from the point of its high electronic conductivity, NiCo₂O₄ has great potential value in the field of absorber with superior dielectric loss[12, 16]. It can be foreseen that various loss mechanisms makes as-prepared samples obtain excellent absorbing performance due to the natural favorable structure, improved impedance matching and optimized conductivity. Furthermore, the finite element simulation of CW@NiCo₂O₄ testifies that horizontal arrangement of the through channels leads to the excellent EMW attenuation ability. Our study provides an alternative strategy to utilize low-priced, environmentally friendly natural wood and simple and efficient preparation procedure to design microwave absorbers with high absorption efficiency and wide absorption frequency. We hope that this work lays a significant foundation for the design and application of wood-derived carbon absorbers to fulfill the ever-growing demands.

2. Experimental

2.1. Preparation of carbonized wood (CW)

All reagents used in our experiments were used as received without further purification.

Poplar wood were purchased from plantation (Hubei China).

To prepare the lignin removal solution, 4g NaClO₂ (80%, Shanghai Macklin Biochemical CO., Ltd) and 1.35ml CH₃COOH (99.5% AR, Tianjin Fuyu Fine Chemical CO., Ltd) were dissolved in 400ml DI water. Then a slice of poplar wood slice cut into 10 mm×10 mm×10 mm was immersed in the as prepared solution in the beaker at 80 °C for 12 h. The lignin-removed wood (LFW) was prepared. Finally, the LFW was placed in a tubular furnace and carbonized at 400 °C under flowing nitrogen for 1.5 h with a heating rate of 3 °C·min⁻¹. The CW was placed in a vacuum drying oven for further use.

2.2. Synthesis of CW@NiCo₂O₄ composites

The CW was immersed in the solution of 1 mol·L⁻¹ of Ni(NO₃)₂·6H₂O and 2 mol·L⁻¹ of Co(NO₃)₂·6H₂O (98% AR, Tianjin Fengchuan Chemical Reagent Technologies CO.,Ltd) in the beaker, then, the beaker was placed in ultrasonic environment for 30 minutes, then allowed to stand for 12 h with -0.1 MPa environment, and finally heated at 50 °C for 6 hours. The CW was fully saturated with Ni(NO₃)₂·6H₂O and Co(NO₃)₂·6H₂O solution. Subsequently, the CW/Ni(NO₃)₂·6H₂O/Co(NO₃)₂·6H₂O composite was placed in a drying oven for 12 h with 60 °C. Finally, the as-obtained material was placed in a tubular furnace for heating to 300 °C for 1 h in air. After the temperature dropped to room temperature, the CW@NiCo₂O₄ hybrid was obtained. For comparison, the CW was also post treated by the same calcination conditions, the post-treated CW was prepared.

2.3. Characterization

Powder XRD pattern was recorded on BRUKER diffractometer using Cu K α radiation. The morphology and microstructure were observed using SEM images on SUPRA™55 (ZEISS, United Kingdom) at high current of 20 kV. The elemental composition was detected by energy dispersive spectrometer (EDS) spectrum deriving from the SEM, coupled with copper grids. Raman spectra were obtained by a Renishaw

Raman microscope using an Ar ion laser (532 nm). Thermogravimetric analysis (TGA) measurements for the composite were carried out by a DTG-60H thermal analyzer under flowing oxygen atmosphere and with a heating rate of 10 °C min⁻¹. The X-ray Photoelectron Spectroscopy (XPS) measurements were recorded on KRATOS Axis Ultra^{DLD} equipped with a monochromatic X-ray source (Al Ka, hv = 1486.6 eV). The room temperature hysteresis loop was performed on vibrating sample magnetometer (VSM, JDAW-2000C&D, Changchun Yingpu CO.,Ltd).

2.4. Electromagnetic parameters measurements

The EM parameters were obtained on vector network analyzer (Agilent, N5230A) by the T/R coaxial line method at 2-18 GHz band. Testing samples of microwave absorption were prepared by cutting method, which can retain the micron-level structure inside the material. Two pieces of CW@NiCo₂O₄ material were respectively tailored into cylindrical toroidal specimens along parallel to the wood growth direction and perpendicular to the wood growth direction (called vertical and horizontal) with an outer diameter of 7.00 mm and inner diameter of 3.00 mm and then were immersed in liquid paraffin wax, after solidification, the sample was prepared, named V-CW@NiCo₂O₄ and H-CW@NiCo₂O₄ respectively. In the same way, the CW material was cut into cylindrical toroidal specimens, named V-CW (vertical) and H-CW (horizontal) respectively. The average filling ratio of coaxial sample was 26 wt% (with the density of 0.98g·cm⁻³) and 21 wt%, respectively, obtained by weighing several times. In addition, the disordered samples (named CW and CW@NiCo₂O₄) were prepared by mixing the powders with paraffin matrix and pressed into a toroidal ring with an outer diameter of 7.00 mm and inner diameter of 3.00 mm with the same filling ratio of ordered-channels samples. The MA performances reflection loss (RL) values were obtained by EM parameters on the basis of transmission line theory, which can be calculated by the following equations based on the metal back-panel model [17, 18].

$$Z_{in} = Z_0 \sqrt{\frac{\mu_r}{\epsilon_r}} \tanh(j2\pi \frac{fd\sqrt{\mu_r\epsilon_r}}{c}) \quad (1)$$

$$RL \text{ (dB)} = 20 \lg \left| \frac{Z_{in} - Z_0}{Z_{in} + Z_0} \right| \quad (2)$$

Here, Z_{in} is the input impedance of absorber, Z_0 is the impedance of free space, ϵ_r and μ_r represent the complex permittivity ($\epsilon_r = \epsilon' - j\epsilon''$) and the complex permeability ($\mu_r = \mu' - j\mu''$), respectively, f indicates the frequency of the incident microwaves, d means the thickness of the microwave absorber, and c is the velocity of the microwave. RL is smaller than -10 dB, it is implied that more than 90% of the microwave is absorbed by MA, and the frequency range can be considered as effective absorption bandwidth (EAB) [19].

3. Results and discussion

The preparation procedure of $CW@NiCo_2O_4$ with the structure of oriented channels and standard coaxial samples was schematically illustrated in Fig. 1.

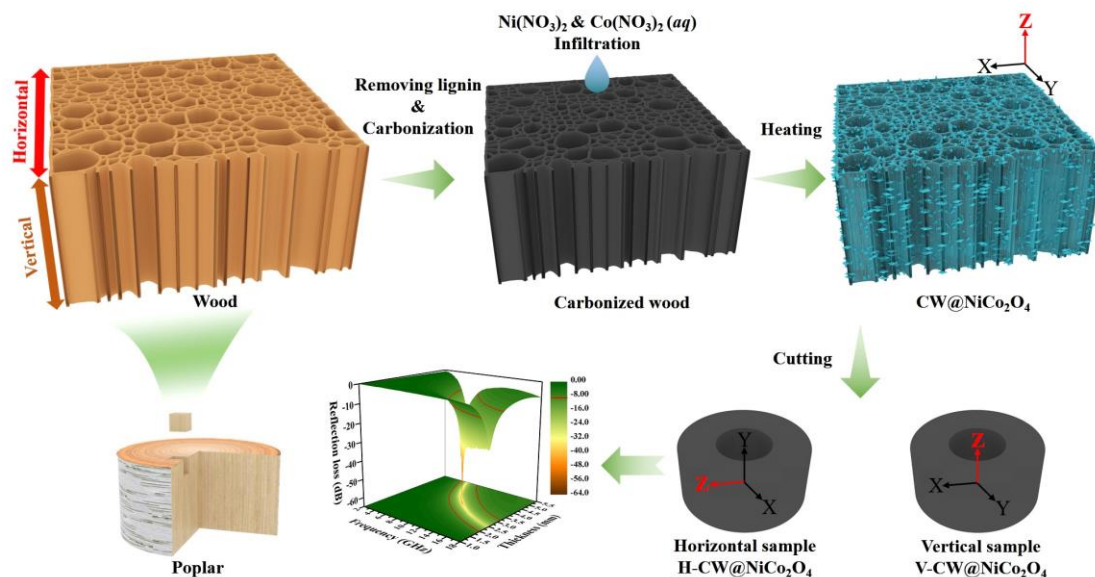


Fig. 1. Fabrication process of $CW@NiCo_2O_4$ with ordered channels, and schematic illustration to obtain vertical and horizontal standard coaxial samples.

The crystallographic structures of CW and $CW@NiCo_2O_4$ were characterized by powder XRD, as shown in Fig. 2a. The broad diffraction peaks at 26.23° and 44.35° correspond to the (200) and (101) crystal planes of graphite crystal structure respectively, indicating that CW is partially graphitized at $400^\circ C$, behaves as amorphous carbon. For the $CW@NiCo_2O_4$ powder sample, the diffraction peaks positions were consistent with the standard XRD patterns of $NiCo_2O_4$ (JCPDS No. 20-0781). The diffraction peaks of $CW@NiCo_2O_4$ composites located at 31.3° , 36.8° , 44.3° , 59.1° and 65.1° could be corresponded to the (220), (311), (400), (511) and (440) crystal planes of $NiCo_2O_4$ phase. Simultaneously, the broad diffraction peaks of amorphous carbon were obtained in the spectrum of $CW@NiCo_2O_4$ composites. These results confirmed that $NiCo_2O_4$ was successfully deposited in through channel of CW. The mass fraction of carbon in $CW@NiCo_2O_4$ composites is obtained by TGA, described in Fig. S1.

Raman spectrum was applied to demonstrate the chemical environment of carbon atoms in the CW and $CW@NiCo_2O_4$ powder, which is an important factor for electron

transportation and make a significant impact on the electromagnetic parameters [20]. In addition, Raman spectrum was also used to characterize the existence of cobalt and nickel atoms. Two obvious peaks located at 1320 cm^{-1} (D band) and 1580 cm^{-1} (G band) can be demonstrated in Fig. 2b. The intensity of the D band peak represents the number of defects or the degree of disorder in the sp^2 -hybridized carbon atoms or amorphous carbon deposits, while the G band peak is associated with the in-plane vibrations of sp^2 atoms in a 2D hexagonal graphitic lattice. The degree of disorder of carbon in the material can be characterized by the ratio of D band to G band (I_D/I_G) [21]. As shown in Fig. 2b, the intensity ratio value of I_D/I_G was 0.85 for CW, and the I_D/I_G value of CW@NiCo₂O₄ was 0.78, which suggested abundant defects exist in both CW and CW@NiCo₂O₄, and the existence of NiCo₂O₄ reduced the degree of disorder of carbon in the material, increased the graphitization degree. The Raman spectrum of spinel Co₃O₄ has a high-frequency peak at 693 cm^{-1} , determined by the octahedral/Co³⁺ [22]. As Co³⁺ was replaced by Ni²⁺, the octahedral/Co³⁺ peak weakens and shifts to lower frequency (Fig. 2b, the band at 650 cm^{-1} of CW@NiCo₂O₄), simultaneously, the octahedral/Ni²⁺ peak was observed at 502 cm^{-1} result from Ni²⁺ substitution at octahedral sites. The peak at 460 cm^{-1} was caused by tetrahedral/Co²⁺. It can be inferred that the Ni²⁺ substitution at octahedral sites would induce the formation of dipole and dipole polarization [22], which is a benefit for EM wave attenuation and thus results in enhanced microwave absorption properties.

The chemical composition and the elemental valence state of the CW@NiCo₂O₄ composites were further characterized by XPS. The wide span spectrum of CW@NiCo₂O₄ composites indicated four typical peaks, corresponding to Ni 2p, Co 2p, O 1s and C 1s, respectively (Fig. 2c). The Ni 2p spectrum has two spin-orbit doublets of Ni²⁺ and Ni³⁺, the binding energies at 854.2, 861.2, 874.4 and 879.6 eV belonged to Ni²⁺, and the peaks at 872.4 eV and 855.8 eV were assigned to Ni³⁺. The binding energies at around 861.3 eV and 879.9 eV were marked to the two shake-up satellite peaks (named as “Sat.”) of nickel (Fig. 2e). Similarly, the Co 2p spectrum given in Fig. 2f consists of one spin-orbit doublet characteristic of Co²⁺ (binding energies at 781.9 and 796.8 eV) and Co³⁺ (binding energies at 779.9 and 795.0 eV) and two shakeup

satellites (binding energies at around 787.9 and 803.7 eV, identified as “Sat.”). The high-resolution C 1s spectrum (Fig. 2d) consisted of three carbon peaks, which represent C-C/C=C (284.7 eV), C-O (285.8 eV) and C=O (288.7 eV), respectively [23]. As shown in Fig. S2, the O 1s spectrum shows three peaks located at 529.5, 531.2, and 532.8 eV, which could be ascribed to the metal–oxygen bonds, defects in oxygen and absorbed water on the surface, respectively [24].

Fig. S3 presents the room temperature hysteresis loops of CW@NiCo₂O₄ (inset: enlarged view at low fields). The magnetization curve performs a typical ferrimagnetic behavior, and the magnetization has been found to not saturate, even at the maximum applied field (10 kOe). The remnant magnetization and coercivity were represented as 0.16 emu·g⁻¹ and 62.5 Oe.

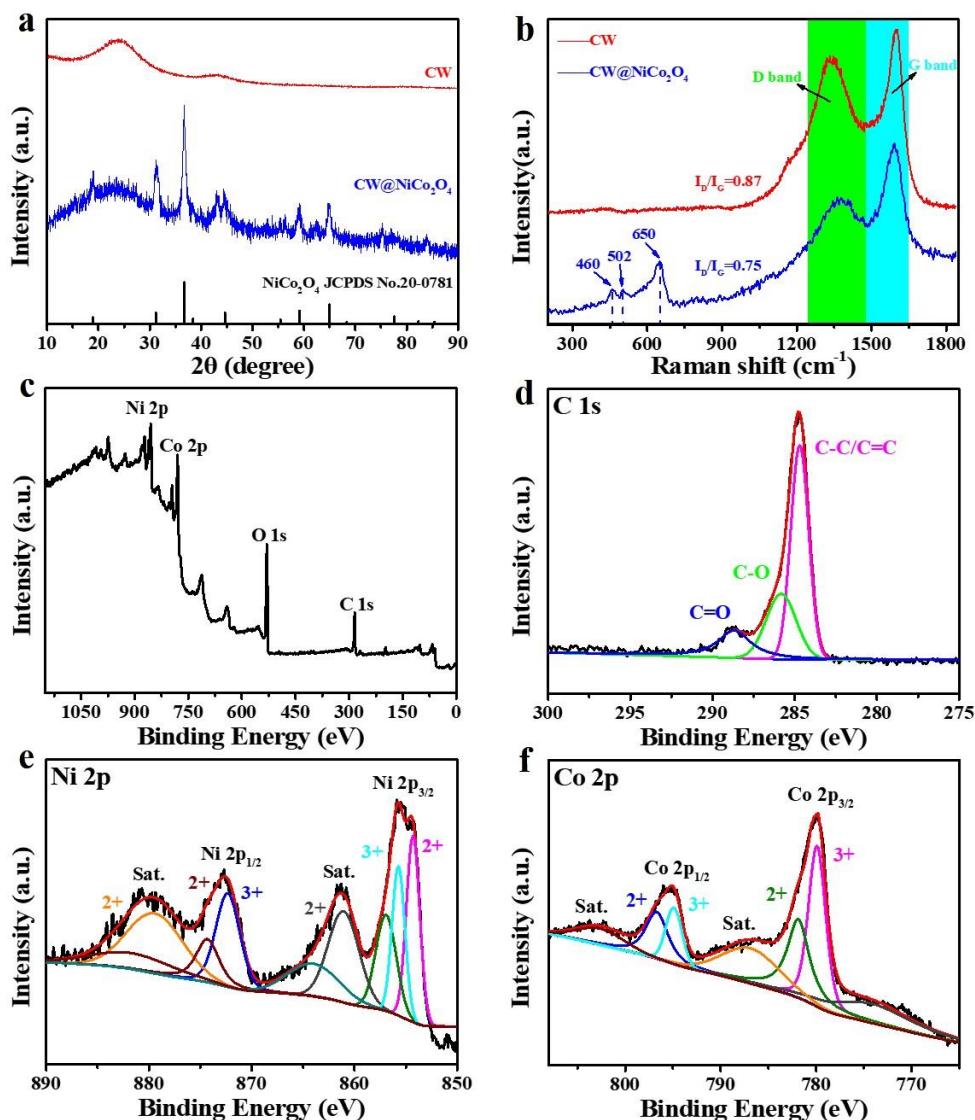


Fig. 2. (a) XRD pattern of CW and CW@NiCo₂O₄; (b) Raman spectra of CW and CW@NiCo₂O₄; XPS spectra of CW@NiCo₂O₄: (c) wide span; (d) C 1s; (e) Ni 2p; (f) Co 2p.

SEM images of CW and CW@NiCo₂O₄ were displayed in Fig. 3. Vertical direction of CW (Fig. 3a) and horizontal direction of CW (Fig. 3b) show that the carbonized wood has through, directional and ordered channels, and the shape of the channels presents an irregular ellipse with a pore size of 10~30 μm and channel wall thickness of 1~3 μm . Vertical direction of CW@NiCo₂O₄ (Fig. 3c) and horizontal direction of CW@NiCo₂O₄ (Fig. 3d) demonstrate that the high-density short cone-like NiCo₂O₄ composites uniformly distributed in the through channels in CW. The thickness of carbon channels wall is obviously thinner than that of CW, because a large

number of carbon atoms are dispersed in the NiCo₂O₄ hybrid in the heat treatment process, which can be further confirmed by energy dispersive X-ray spectroscopy (EDS) mapping images (Fig. S4). An image in the inset of Fig. 3c reveals that the magnified cone-like C/NiCo₂O₄. Simultaneously, the through, directional and ordered channels were retained in the CW@NiCo₂O₄, this unique ordered pore microstructure can enable abundant multiple reflections of electromagnetic waves and interfacial polarization, which are favorable for the microwave absorption performance.

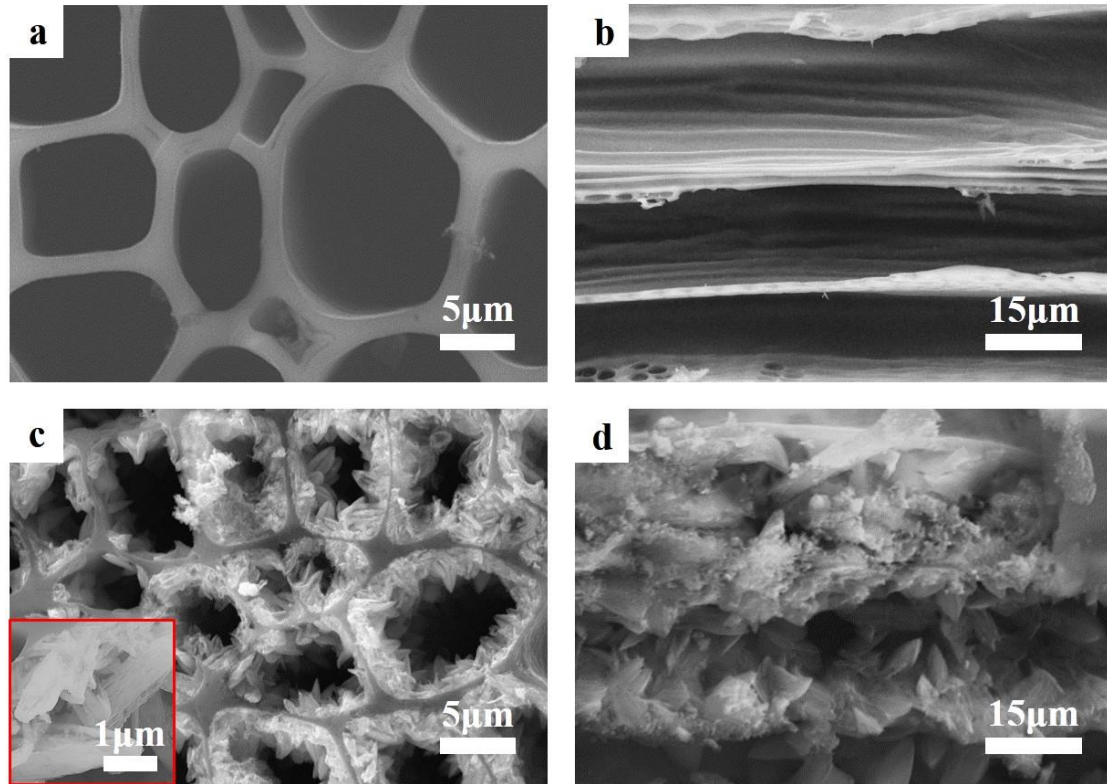


Fig. 3. SEM images of (a) V-CW, (b) H-CW, (c) V-CW@NiCo₂O₄, (d) H-CW@NiCo₂O₄.

Generally, the hybrid magnetic/dielectric composites present excellent EMW absorption capabilities due to electromagnetic complementation and impedance matching effects. Our ordered-channel CW@NiCo₂O₄ composites with unique microstructure perform excellent microwave absorption abilities. Impedance matching ratio ($|Z_{in} / Z_0|$) is also an important parameter for EMW absorption. The impedance characteristic of the absorber close to that of free space (the value of $|Z_{in} / Z_0|$ close to 1), which means that the incident EMW can enter the absorber to the greatest extent[16]. Fig. S5 presents the RL curves and impedance matching ratio of V-CW, H-

CW and V-CW@NiCo₂O₄ samples with thickness from 1.0 to 5.5 mm in the frequency range of 2.0-18.0 GHz. It is observed that these three samples showed almost no microwave absorption (Fig. S5a, S5b and S5c), result from poor impedance matching performance. Nevertheless, as shown in Fig. S5d, S5e and S5f, the impedance matching performance of the three samples were found to be quite different. The impedance matching ratio of H-CW and V-CW@NiCo₂O₄ are closer to 1 than that of V-CW, which implies that the through-channels arranged horizontally relative to the incident direction of electromagnetic waves have better impedance matching performance than those arranged vertically, are more conducive to electromagnetic wave loss, and that the NiCo₂O₄ was introduced in through channels also achieves the same effect. The RL value and impedance matching ratio of disordered CW and CW@NiCo₂O₄ samples demonstrated similar laws (Fig. S6). The sample of H-CW@NiCo₂O₄ composites exhibited excellent EMW absorption capabilities with the NiCo₂O₄ distributed in through-channels arranged horizontally. As observed from Fig. 4c, the sample of H-CW@NiCo₂O₄ reaches a strong absorption intensity of -64.02 dB at 10.72 GHz with the thickness of 3.62 mm, and the corresponding EAB value is 6.08GHz (8.48-14.56GHz). In particular, the maximum EAB value for the sample is 8.08 GHz (9.92-18.0 GHz) at the thickness of 3.2 mm, the super-wide EAB value could cover the entire Ku-band and the most X-band. We compare the performance of the H-CW@NiCo₂O₄ sample to some similar materials reported in previous reports, the result is shown in Table 1. The excellent performance of RL, EAB and thickness value clearly demonstrate the natural wood-derived carbon has great potential for microwave absorption. Unsurprisingly, the H-CW@NiCo₂O₄ exhibits superior impedance matching at 2-5.5 mm thicknesses range with $|Z_{in} / Z_0|$ values between 0.75 and 1.25 in the 5-18 GHz range (Fig. 4a). Moreover, it is obvious that the RL peaks move to the lower frequency region as the thickness increased. This result can be explained by quarter-wavelength attenuation law, which means that when the absorber reaches the matching thickness (t_m), the reflected waves derived from the upper and bottom interface are out of phase by 180° and completely cancel each other in the air-absorber interface [25]:

$$t_m = \frac{n}{4} \lambda = \frac{nc}{4f\sqrt{|\mu_r \epsilon_r|}} \quad (n = 1, 3, 5, \dots) \quad (3)$$

Here, t_m is the matching thickness and λ , f , and c represent the wavelength, frequency, and velocity of the microwave, respectively. Obviously, the t_m values of the H-CW@NiCo₂O₄ are basically consistent with the curve of quarter-wavelength attenuation model. What's more, by comparing the values of the $|Z_{in} / Z_0|$ and RL curve, the close correlation between them can clearly be found, that is, the closer the value of $|Z_{in} / Z_0|$ is to 1, the greater the RL value.

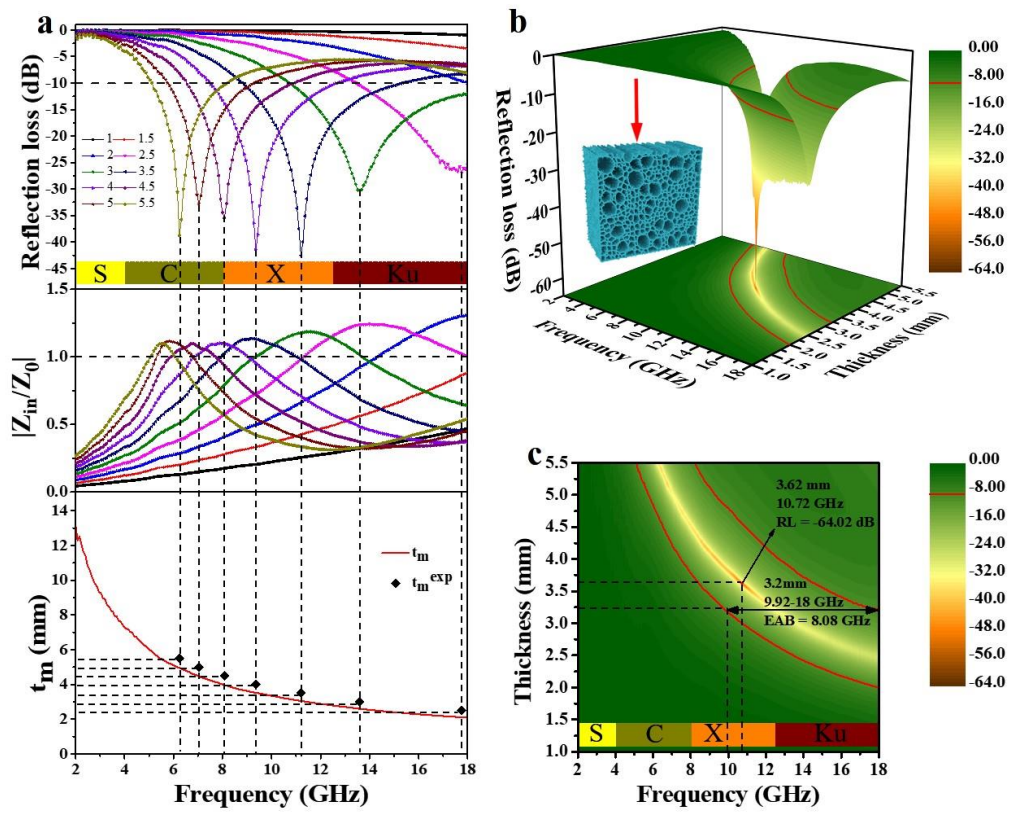


Fig. 4. RL value, impedance matching ratio, actual thickness t_m^{exp} and calculated thickness t_m for (a) H-CW@NiCo₂O₄; (b) 3D RL value and (c) contour map of H-CW@NiCo₂O₄.

Table 1. Microwave absorption performance of some carbonized wood-based materials.

Sample	Filling ratio	RL _{min} /Thickness	EAB _{max}	Reference
PBPC ^a	-	-68.3 dB/4.28mm	7.63 GHz	[13]
NiCo ₂ S ₄ /C	50 wt%	-64.7 dB/1.91mm	5.26 GHz	[10]
FeCo/C@WC ^b	85 wt%	-47.6 dB/1.5mm	8.9 GHz	[26]
CoFe/BPC ^c	-	-53.6dB/2.2mm	2.7 GHz	[27]
H-CW@NiCo ₂ O ₄	26 wt%	-64.0 dB/3.62mm	8.08 GHz	This work

^aPBPC: Porous biomass-pyrolyzed carbon; ^b WC: wood carbon aerogel; ^c BPC: biomass porous carbon

Generally speaking, the MA properties is not only controlled by impedance matching characteristics, but also affected by the attenuation energy capacity. Attenuation capacity is explained by that, EMW is converted into other forms of energy inside absorber due to the existence of various loss mechanisms, such as conductivity loss, polarization loss, natural resonance or eddy current loss, calculated as the attenuation constant (α) [28]:

$$\alpha = \frac{\sqrt{2}\pi f}{c} \sqrt{(\mu''\varepsilon'' - \mu'\varepsilon') + \sqrt{(\mu''\varepsilon'' - \mu'\varepsilon')^2 + (\mu'\varepsilon'' + \mu''\varepsilon')^2}} \quad (4)$$

From Fig. 6a, it can be observed that the H-CW@NiCo₂O₄ sample shows the largest of values attenuation constant α , almost above 100 in the 2-18 GHz frequency range, indicating the stronger microwave attenuation ability of the H-CW@NiCo₂O₄ sample than that of the other three samples, result from the NiCo₂O₄ distributed in through-channels arranged horizontally. In addition, as a whole, the introduction of NiCo₂O₄ promoted the increase in attenuation capacity.

In order to explain the microwave absorption mechanisms of as-prepared materials, the complex permittivity (ε' , ε''), permeability (μ' , μ''), dielectric tangent loss ($\tan \delta_e = \varepsilon'' / \varepsilon'$) and magnetic tangent loss ($\tan \delta_m = \mu'' / \mu'$) are shown in Fig. 5. the real parts (ε' and μ') represent the stored capability of electric and magnetic energy while the imaginary parts (ε'' and μ'') represent the dissipated capability of electric and magnetic energy, respectively. $\tan \delta_e$ and $\tan \delta_m$ represent dielectric and magnetic loss capacities of the absorber, respectively [29]. From Fig. 5a and 5b, it is observed that the ε' and ε'' values of the H-CW@NiCo₂O₄ greater than that of the other three samples, and possess a decreased

trend as the frequency increases, which is attributed to the increased polarization hysteresis versus the higher frequency electric-field variation [30]. As for V-CW@NiCo₂O₄ sample, its ϵ' and ϵ'' values are slightly higher than that of V-CW and H-CW, and basically do not change with the increase of frequency, showing a horizontal line relative to the frequency. The ϵ' values of V-CW and H-CW are the lowest, stay near 2 and do not change with frequency and the ϵ'' values behave the same trend as ϵ' . The calculated $\tan \delta_e$ of all samples were depicted in Fig. 5c. The curve of $\tan \delta_e$ value for the H-CW@NiCo₂O₄ sample shows a trend of small fluctuations between 0.4 and 0.6, and the values clearly higher than the other samples. As for other three samples, the trend of $\tan \delta_e$ value is similar to that of ϵ'' results shown in Fig. 5b. The H-CW@NiCo₂O₄ sample presents the largest $\tan \delta_e$ value in 2-18 GHz frequency range compared with the other samples, demonstrating the best dielectric loss performance.

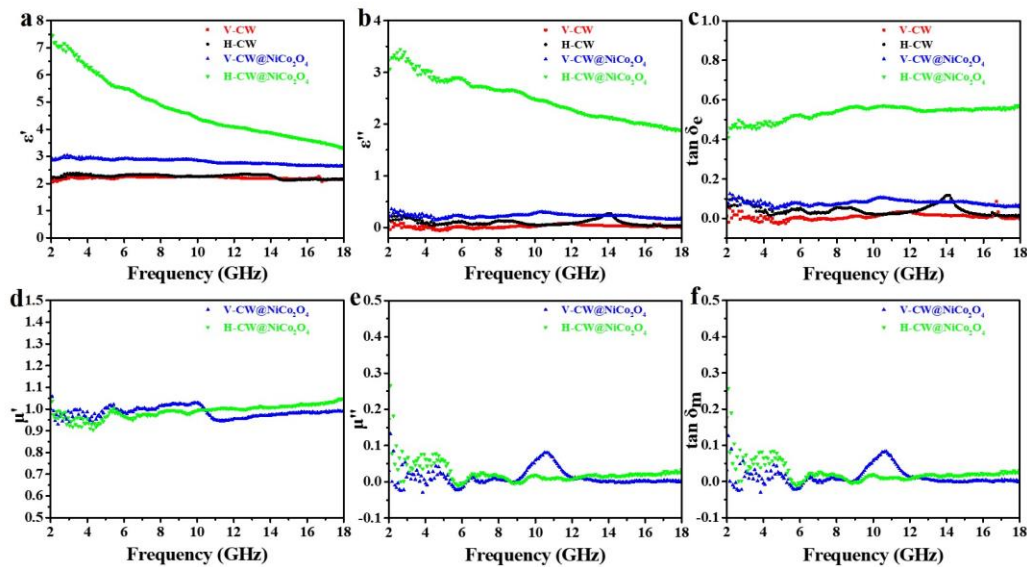


Fig. 5. The EM parameters of samples: (a) real part ϵ' and (b) imaginary part ϵ'' of permittivity, (c) dielectric loss $\tan \delta_e$, (d) real part μ' and (e) imaginary part μ'' of permeability, (f) magnetic loss $\tan \delta_m$.

Generally speaking, the dielectric loss is closely associated with conductive loss and polarization loss, and the conductive loss lies on the electrical conductivity [31]. The introduction of NiCo₂O₄ could effectively enhance the conductive loss result from the high electrical conductivity. In detail, the NiCo₂O₄ hybrid uniformly

distributed in the through channels formed by amorphous carbon, which allows the CW@NiCo₂O₄ composites to form an efficient conductive network, which could be confirmed by the ε'' curves of as-prepared samples, the ε'' values of CW@NiCo₂O₄ composites are higher than that of single CW. Simultaneously, the H-CW@NiCo₂O₄ sample displays the greatest conductive loss capacity. The polarization loss comes from atomic polarization, electron polarization, dipole polarization and interfacial polarization [32]. The atomic polarization and electron polarization could be eliminated firstly, because these two polarizations could only appear at higher frequency range. The dielectric loss for as-prepared samples should be mostly ascribed to the dipole polarization, which can be explained by the Cole-Cole model [33-35]:

$$\varepsilon_r = \varepsilon' - j\varepsilon'' = \varepsilon_\infty + \frac{\varepsilon_s - \varepsilon_\infty}{1 + j2\pi f\tau} \quad (5)$$

Here, ε_s , ε_∞ , f and τ stands for the static dielectric constant, the dielectric constant at infinite frequency, the frequency and the polarization relaxation time, respectively. And then the ε' and ε'' can be expressed as:

$$\varepsilon' = \varepsilon_\infty + \frac{\varepsilon_s - \varepsilon_\infty}{1 + (2\pi f)^2\tau^2} \quad (6)$$

$$\varepsilon'' = \frac{2\pi f\tau(\varepsilon_s - \varepsilon_\infty)}{1 + (2\pi f)^2\tau^2} \quad (7)$$

Consequently, the relationship between ε' and ε'' can be depicted as:

$$\left(\varepsilon' - \frac{\varepsilon_s + \varepsilon_\infty}{2}\right)^2 + (\varepsilon'')^2 = \left(\frac{\varepsilon_s - \varepsilon_\infty}{2}\right)^2 \quad (8)$$

Therefore, the relationship between ε' and ε'' can be determined as a single semicircle, called the Cole-Cole semicircle, each Cole-Cole semicircle represents a Debye dipolar relaxation process. Fig. 6c, 6d and Fig. S7 demonstrates the Cole-Cole curves of all tested samples in the 2-18 GHz frequency range. As mentioned above, enhancement of the Debye dipolar relaxation is definitely reflected in the increasing number of semicircles [36, 37]. As for V-CW and H-CW (Fig. S7), the points on the curves are concentrated in a small range, which will lead to the existence of a large number of Cole-Cole semicircles. It can be inferred that the numerous defects within the CW were served as the polarization centers to promote the formation of Debye

dipole polarization, which could be confirmed by the result of I_D/I_G value in Fig. 2b. However, the strongest Debye relaxation of CW results in extremely poor conductivity and eventually leads to improper impedance matching. The existence of NiCo_2O_4 not only reduces the I_D/I_G value of CW (Fig. 2b) to improve conductivity and impedance matching, but also causes interface polarization to increase the dielectric loss capability. The number of Cole-Cole semicircles is reduced to a level that can be basically identified in the Cole-Cole curves of $\text{H-CW@NiCo}_2\text{O}_4$ and $\text{V-CW@NiCo}_2\text{O}_4$ samples, which implies the dielectric loss for $\text{CW@NiCo}_2\text{O}_4$ hybrid composites should not mainly come from the Debye dipolar relaxation, and the conductive loss and interfacial polarization should play dominant role in dielectric loss.

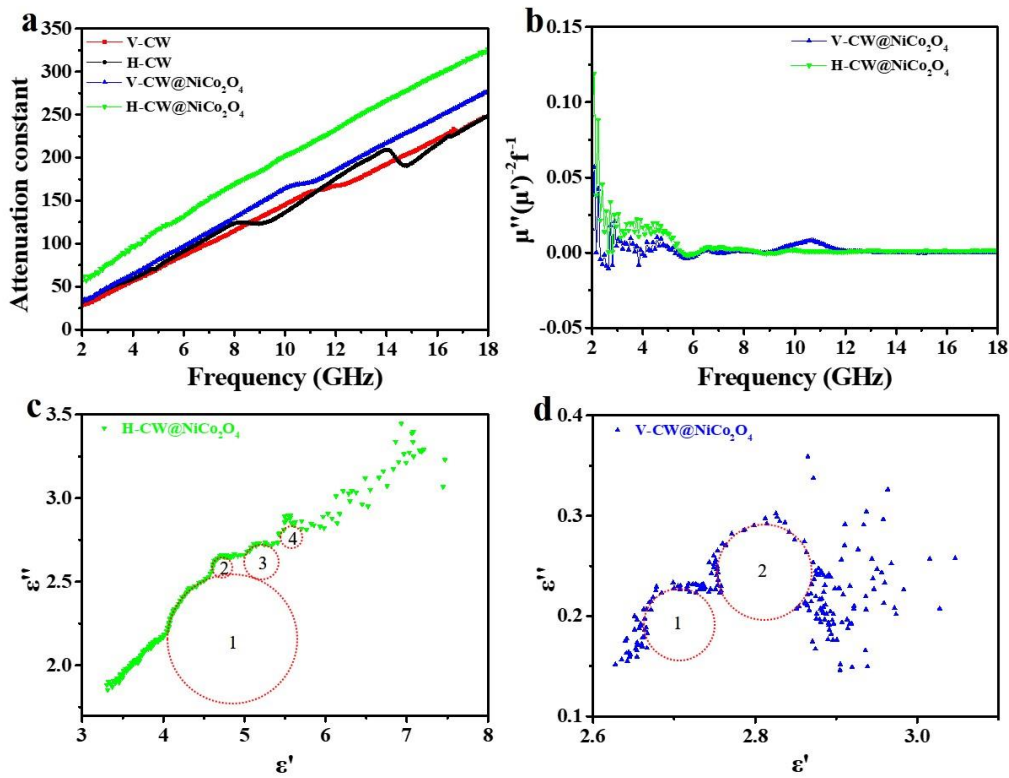


Fig. 6. (a) Attenuation constant α of all samples, (b) C_0 values versus frequency of $\text{V-CW@NiCo}_2\text{O}_4$ and $\text{H-CW@NiCo}_2\text{O}_4$, Cole-Cole curves of (c) $\text{H-CW@NiCo}_2\text{O}_4$ and (d) $\text{V-CW@NiCo}_2\text{O}_4$.

Fig. 5d and 5e present the changes of complex permeability in the frequency range of 2-18 GHz for the $\text{H-CW@NiCo}_2\text{O}_4$ and $\text{V-CW@NiCo}_2\text{O}_4$ samples. The μ' and μ'' intensively slightly fluctuated with frequency, and varied in the range of

0.90–1.05 and 0–0.17, respectively. Meanwhile, the values of the calculated dielectric loss tangent $\tan \delta_m$ of these two samples were depicted in Fig. 5f, the values are almost below 0.2, and there is no obvious resonance peak appears on the curves, which means that the magnetic loss does not contribute much to the MA performance. In general, magnetic loss mainly result from natural resonance, exchange resonance and eddy current loss in the microwave frequency bands [38].

Here, the low-frequency resonance is mainly assigned to the natural resonance, while the exchange resonance almost takes place at higher frequencies [39]. The eddy current loss effect could be demonstrated by the C_0 curve [40]:

$$C_0 = \frac{\mu''}{(\mu')^2 f} \quad (8)$$

If the eddy current loss is the dominated factor for the magnetic loss, the value of C_0 should be a constant, which makes the C_0 value appear as a horizontal line in $C_0 - f$ curve. As shown in Fig. 6b, in 2-7 GHz frequency range, the noticeable resonance peaks can be detected, which is assigned to natural resonance. The C_0 curve of H-CW@NiCo₂O₄ is nearly never change in the frequency range of 7-18 GHz, while a tiny resonance peak was found in the C_0 curve of V-CW@NiCo₂O₄ at 10.5 GHz. The great difference of MA performance between H-CW@NiCo₂O₄ and V-CW@NiCo₂O₄ samples is discovered in Fig. 4 and Fig. S5c, while the magnetic parameters of them behave basically similar, which implies that the dielectric loss controlled by microstructure and composition is the main influence factor on absorbing electromagnetic wave.

In order to explore the influence of the arrangement direction of ordered channels on the performance of MA, the two channel arrangement directions of CW@NiCo₂O₄ composite were constructed as simplified models for finite element analysis (FEA) simulation. The simplified model of V-CW@NiCo₂O₄ is demonstrated in Fig. 7, with the channel diameter and channel wall thickness set to 10 μm and 3 μm , respectively, which is derived from the SEM pictures of actual structure shown in Fig. 3c and 3d. In addition, the inside of the channels is filled with paraffin wax, and the section to be explored is marked in the model diagram. The frequency parameter

of the simulation calculation process was set to 10.72GHz. The time-average power flow ($poav$) of section 1 and section 2 are shown in Fig. 7b and Fig. 7c, respectively. The $poav$ can be regarded as the propagation path and energy distribution of EMW inside the material, which is reflected in the direction and size of $poav$ arrow. Obviously, the vertical channel is less obstructive to the EMW, and the EMW can easily pass through the channel without sufficient interaction with the material. Furthermore, Fig. 7d, 7e and 7f proves that V-CW@NiCo₂O₄ composite has little attenuation ability to EMW. As for H-CW@NiCo₂O₄, the transmission direction and intensity of EMW change significantly near the channels wall (Fig. 8b), which indicates that the material has an effective interaction with microwave, due to multiple reflection and scattering caused by ordered porous structure. Simultaneously, as shown in Fig. 8c, 8d and 8e, strong dielectric loss occurs near the channels wall, result from the high-efficiency conductive network formed by carbonized wood decorated with NiCo₂O₄ hybrids and polarization relaxation. It is worth noting that the intensity distributions of total loss power density (Fig. 8c) and dielectric loss power density (Fig. 8d) are very similar and the intensity of magnetic loss power density (Fig. 8e) is extremely low compared to dielectric loss power density. In other words, the contribution of magnetic loss to MA is extremely small compared to dielectric loss, this result is consistent with the previous analysis of EM parameters.

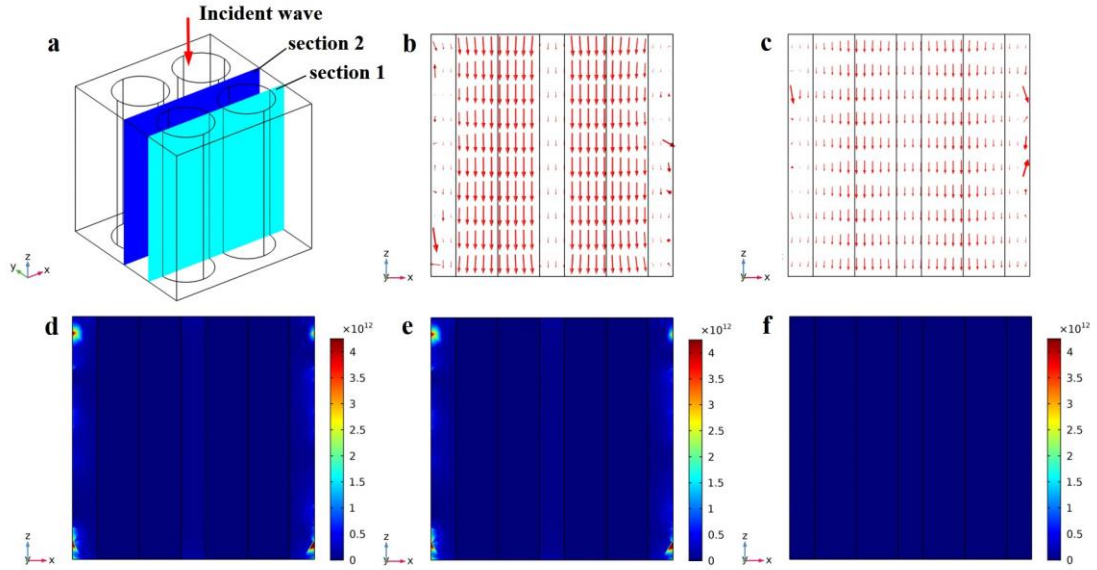


Fig. 7. The FEA simulation of V-CW@NiCo₂O₄. (a) Schematic diagram of simplified model and sections position; The (b) time-average power flow $poav$ ($W \cdot m^{-2}$), (d) total loss power density Q ($W \cdot m^{-3}$), (e) dielectric loss power density Q_e ($W \cdot m^{-3}$), and (f) magnetic loss power density Q_m ($W \cdot m^{-3}$) in section 1; (c) The time-average power flow $poav$ ($W \cdot m^{-2}$) in section 2.

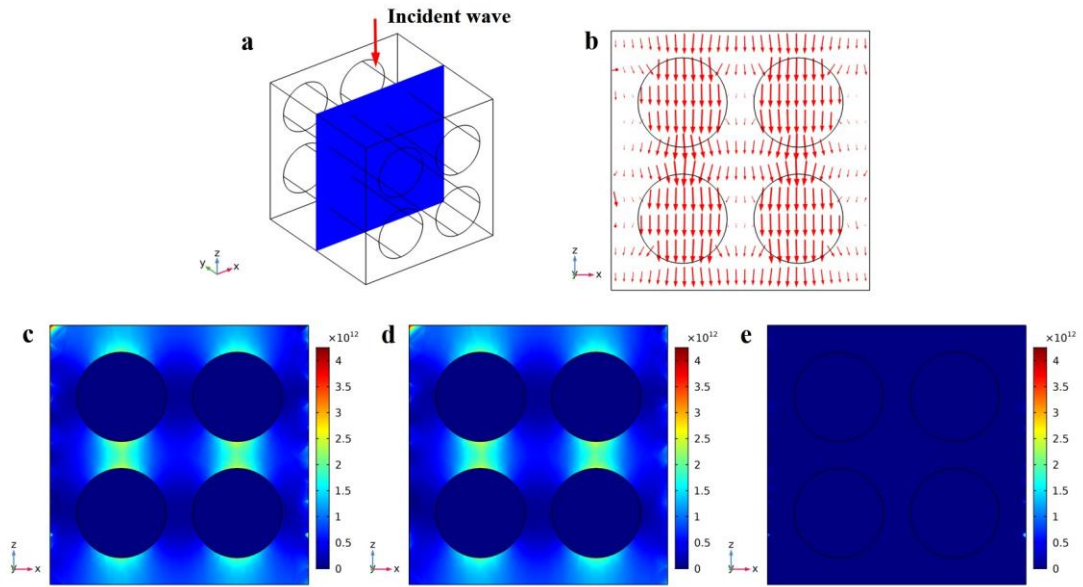


Fig. 8. The FEA simulation of H-CW@NiCo₂O₄. (a) Schematic diagram of simplified model and section position; The (b) time-average power flow $poav$ ($W \cdot m^{-2}$), (c) total loss power density Q ($W \cdot m^{-3}$), (d) dielectric loss power density Q_e ($W \cdot m^{-3}$), and (e) magnetic loss power density Q_m ($W \cdot m^{-3}$) in section 1.

In summary, the possible MA mechanism of the H-CW@NiCo₂O₄ hybrid composites is described in Fig. 9. Firstly, the NiCo₂O₄ hybrids infiltrated into a large number of carbon atoms are uniformly distributed on the wall of the ordered channels, result in the conductivity of the material is effectively enhanced, so that the 3D conductive skeleton derived from natural wood would promote the electron transportation and improve the dielectric loss ability. Secondly, the interface between carbon and NiCo₂O₄ would form non-uniform charge distribution and interfacial polarization loss, because of the difference of electrical conductivity. Thirdly, the presence of defects within the amorphous carbon and NiCo₂O₄ hybrids would serve as the polarization centers to induce the multiple reflection and scattering processes. Fourthly, the magnetic loss including natural resonance and eddy current loss should also contribute to the microwave absorption property to a slight extent. Therefore, benefiting from the matched impedance and the enhanced attenuation constant, the carbonized wood with horizontally ordered channels decorated by cone-like NiCo₂O₄ hybrids (H-CW@NiCo₂O₄) cause the outstanding MA performance.

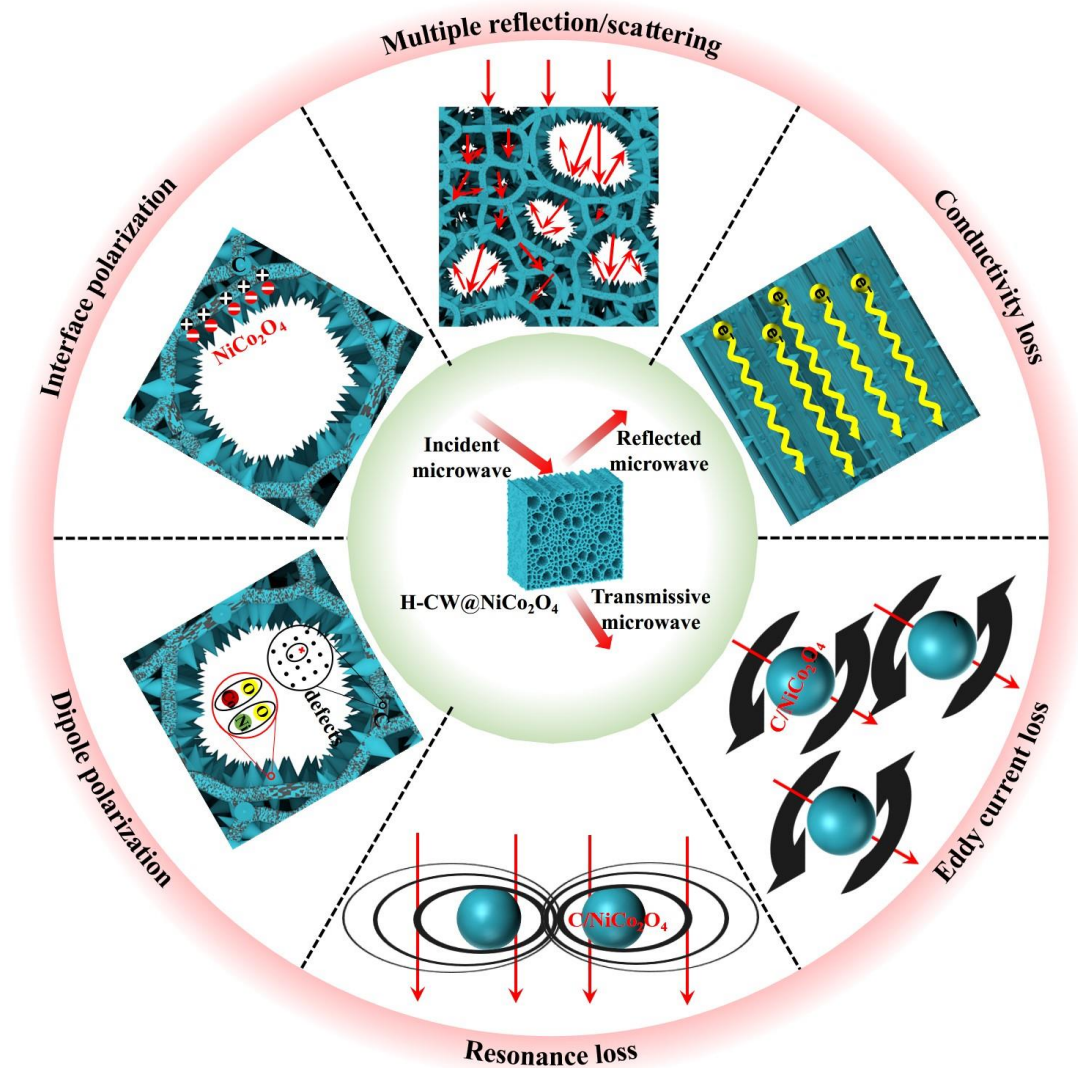


Fig. 9. Schematic illustration for the EMW absorption of H-CW@NiCo₂O₄.

Conclusion

This work reported a wood-derived carbon-based material with ordered channels decorated by NiCo₂O₄ hybrids, which is manufactured through a facile, low-cost and sustainable method with outstanding EMW absorption performance. The combination of 3D carbon skeleton with horizontal ordered channels derived from natural wood and NiCo₂O₄ hybrids together enable multiple EMW loss mechanisms to be effectively realized, resulting in the matched impedance and the enhanced attenuation constant. The horizontal arrangement of the through channels of CW@NiCo₂O₄ (H-CW@NiCo₂O₄) exhibits a strong reflection loss value of -64.0 dB at 10.72 GHz with a thickness of 3.62 mm and a low filling ratio of 26%, and the effective absorption

bandwidth (EAB) is 8.08 GHz (9.92-18.0 GHz) at the thickness of 3.2 mm. The result of finite element analysis (FEA) simulation confirms that the horizontal arrangement of ordered channels allows the material to interact effectively with electromagnetic waves, thereby obtaining excellent MA property. This research provides a facile and novel strategy for using carbonized wood to fabricate advanced microwave absorbers with lightweight and strong attenuation capabilities.

Acknowledgements

This work was supported by National Natural Science Foundation of China (NSFC 51772060, 51372052 and 51621091).

References

- [1] Wang FY, Wang N, Han XJ, *et al.* Core-shell FeCo@carbon nanoparticles encapsulated in polydopamine-derived carbon nanocages for efficient microwave absorption. *Carbon* 2019, **145**: 701-711.
- [2] Yan J, Huang Y, Chen C, *et al.* The 3D CoNi alloy particles embedded in N-doped porous carbon foams for high-performance microwave absorbers. *Carbon* 2019, **152**: 545-555.
- [3] Pang YQ, Li Yf, Wang JF, *et al.* Carbon fiber assisted glass fabric composite materials for broadband radar cross section reduction. *Compos. Sci. Technol.* 2018, **158**: 19-25.
- [4] Arjmand M, Chizari K, Krause B, *et al.* Effect of synthesis catalyst on structure of nitrogen-doped carbon nanotubes and electrical conductivity and electromagnetic interference shielding of their polymeric nanocomposites. *Carbon* 2016, **98**: 358-372.
- [5] Li F, Zhan WW, Su YT, *et al.* Achieving excellent electromagnetic wave absorption of ZnFe₂O₄@CNT/polyvinylidene fluoride flexible composite membranes by adjusting processing conditions. *Compos. Pt. A-Appl. Sci. Manuf.* 2020, **133**.
- [6] Shi YA, Gao XH, Qiu J. Synthesis and strengthened microwave absorption properties of three-dimensional porous Fe₃O₄/graphene composite foam. *Ceram. Int.* 2019, **45**(3): 3126-3132.
- [7] Xiong CY, Li BB, Liu HG, *et al.* A smart porous wood-supported flower-like NiS/Ni conjunction with vitrimer co-effect as a multifunctional material with reshaping, shape-memory, and self-healing properties for applications in high-performance supercapacitors, catalysts, and sensors. *J. Mater. Chem. A* 2020, **8**(21): 10898-10908.
- [8] Zhang WY, Yang YN, Xia RQ, *et al.* Graphene-quantum-dots-induced MnO₂ with needle-like nanostructure grown on carbonized wood as advanced electrode for supercapacitors. *Carbon* 2020, **162**: 114-123.
- [9] Chen BL, Gsalla A, Gaur A, *et al.* Porous wood monoliths decorated with platinum nano-urchins as catalysts for underwater micro-vehicle propulsion via H₂O₂ decomposition. *ACS Appl. Nano Mater.* 2019, **2**(7): 4143-4149.
- [10] Dong S, Hu PT, Li XT, *et al.* NiCo₂S₄ nanosheets on 3D wood-derived carbon for microwave absorption. *Chem. Eng. J.* 2020, **398**.
- [11] Zheng Y, Song YJ, Gao T, *et al.* Lightweight and hydrophobic three-dimensional wood-derived anisotropic magnetic porous carbon for highly efficient electromagnetic interference shielding. *ACS Appl. Mater. Interfaces* 2020, **12**(36): 40802-40814
- [12] Wei SA, Wang XX, Zhang BQ, *et al.* Preparation of hierarchical core-shell C@NiCo₂O₄@Fe₃O₄ composites for enhanced microwave absorption performance. *Chem. Eng. J.* 2017, **314**: 477-487.
- [13] Xi JB, Zhou EZ, Liu, YJ, *et al.* Wood-based straightway channel structure for high performance microwave absorption. *Carbon* 2017, **124**: 492-498.
- [14] Dhavale SB, Patil VL, Beknalkar SA, *et al.* Study of solvent variation on controlled synthesis of different nanostructured NiCo₂O₄ thin films for supercapacitive application. *J. Colloid Interface Sci.* 2021, **588**: 589-601.

- [15] Jang KB, Park KR, Kim KM, *et al.* Electrochemical performance of the spinel NiCo₂O₄ based nanostructure synthesized by chemical bath method for glucose detection. *Appl. Surf. Sci.* 2021, **545**.
- [16] Liu XF, Hao CC, Jiang. H, *et al.* Hierarchical NiCo₂O₄/Co₃O₄/NiO porous composite: a lightweight electromagnetic wave absorber with tunable absorbing performance. *J. Mater. Chem. C* 2017, **5**(15): 3770-3778.
- [17] Zhao HB, Cheng JB, Zhu JY, *et al.* Ultralight CoNi/rGO aerogels toward excellent microwave absorption at ultrathin thickness. *J. Mater. Chem. C* 2019, **7**(2): 441-448.
- [18] Yan X, Huang XX, Chen YT, *et al.* A theoretical strategy of pure carbon materials for lightweight and excellent absorption performance. *Carbon* 2021, **174**: 662-672.
- [19] Xu W, Wang GS, Yin PG. Designed fabrication of reduced graphene oxides/Ni hybrids for effective electromagnetic absorption and shielding. *Carbon* 2018, **139**: 759-767.
- [20] Wang L, Yu XF, Li X, *et al.* Conductive-network enhanced microwave absorption performance from carbon coated defect-rich Fe₂O₃ anchored on multi-wall carbon nanotubes. *Carbon* 2019, **155**: 298-308.
- [21] Wang X, Pan F, Xiang Z, *et al.* Magnetic vortex core-shell Fe₃O₄@C nanorings with enhanced microwave absorption performance. *Carbon* 2020, **157**: 130-139.
- [22] Wu HJ, Wu GL, Ren YY, *et al.* Co²⁺/Co³⁺ ratio dependence of electromagnetic wave absorption in hierarchical NiCo₂O₄-CoNiO₂ hybrids. *J. Mater. Chem. C* 2015, **3**(29): 7677-7690.
- [23] Qin ZH, Wang CY, Wang JJ, *et al.* Spherical shape Co@Co₃O₄ core-shell composites grown on surface of graphite nanosheets with ultra-thin and excellent electromagnetic absorption performance. *Appl. Surf. Sci.* 2021, **539**.
- [24] Xu XQ, Ran FT, Fan ZM, *et al.* Bimetallic metal-organic framework derived pomegranate-like nanoclusters coupled with CoNi doped graphene for strong wideband microwave absorption. *ACS Appl. Mater. Interfaces* 2020, **12**(15): 17882-17892.
- [25] Wu HJ, Zhao ZH, Wu GL. Facile synthesis of FeCo layered double oxide/raspberry-like carbon microspheres with hierarchical structure for electromagnetic wave absorption. *J. Colloid Interface Sci.* 2020, **566**: 21-32.
- [26] Xiong Y, Xu LL, Yang CX, *et al.* Implanting FeCo/C nanocages with tunable electromagnetic parameters in anisotropic wood carbon aerogels for efficient microwave absorption. *J. Mater. Chem. A* 2020, **8**(36): 18863-18871
- [27] Ji C, Liu Y, Li YY, *et al.* Facile preparation and excellent microwave absorption properties of cobalt-iron/porous carbon composite materials. *J. Magn. Magn. Mater.* 2021, **527**.
- [28] Liu PB, Gao S, Wang Y, *et al.* Core-shell Ni@C encapsulated by N-doped carbon derived from nickel-organic polymer coordination composites with enhanced microwave absorption. *Carbon* 2020, **170**: 503-516.
- [29] Wang Y, Di XC, Lu Z. Controllable construction design of Co@C@MWCNTs interpenetrating composite with tunable enhanced electromagnetic wave absorption. *J.*

- Mater. Sci.-Mater. Electron.* 2021, **32**(1): 1061-1072.
- [30] Wang JW, Wang BB, Feng AL, *et al.* Design of morphology-controlled and excellent electromagnetic wave absorption performance of sheet-shaped ZnCo₂O₄ with a special arrangement. *J. Alloy. Compd.* 2020, **834**.
- [31] Dong S, Zhang WZ, Zhang XH, *et al.* Designable synthesis of core-shell SiCw@C heterostructures with thickness-dependent electromagnetic wave absorption between the whole X-band and Ku-band. *Chem. Eng. J.* 2018, **354**: 797-779
- [32] Zhang HX, Jia ZR, Feng AL, *et al.* Enhanced microwave absorption performance of sulfur-doped hollow carbon microspheres with mesoporous shell as a broadband absorber. *Compos. Commun.* 2020, **19**: 42-50.
- [33] Zhang MM, Jiang ZY, Si HX, *et al.* Heterogeneous iron–nickel compound/RGO composites with tunable microwave absorption frequency and ultralow filler loading. *Phys. Chem. Chem. Phys.* 2020, **22**(16): 8639-8646.
- [34] Wang XY, Lu YK, Zhu T, *et al.* CoFe₂O₄/N-doped reduced graphene oxide aerogels for high-performance microwave absorption. *Chem. Eng. J.* 2020, **388**.
- [35] Yan X, Huang XX, Bo Z, *et al.* Balancing interface polarization strategy for enhancing electromagnetic wave absorption of carbon materials. *Chem. Eng. J.* 2020, **391**.
- [36] Chen JP, Jia H, Liu Z, *et al.* Construction of C-Si heterojunction interface in SiC whisker/reduced graphene oxide aerogels for improving microwave absorption. *Carbon* 2020, **164**: 59-68.
- [37] Gao F, Xie WS, Miao YQ, *et al.* Magnetic hydrogel with optimally adaptive functions for breast cancer recurrence prevention. *Adv. Healthc. Mater.* 2019, **8**(14).
- [38] Lyu N, Wang JH, Shen HJ, *et al.* Graphene quantum dots interfacial-decorated hierarchical Ni/PS core/shell nanocapsules for tunable microwave absorption. *J. Alloy. Compd.* 2020, **848**.
- [39] Zhang X, Qiao J, Zhao JB, *et al.* High-efficiency electromagnetic wave absorption of cobalt-decorated NH₂-UIO-66 derived porous ZrO₂/C. *ACS Appl. Mater. Interfaces* 2019, **11**(39): 35959-35968.
- [40] Yu JY, Chi FL, Sun YP, *et al.* Assembled porous Fe₃O₄@g-C₃N₄ hybrid nanocomposites with multiple interface polarization for stable microwave absorption. *Ceram. Int.* 2018, **44**(16): 19207-19216.

Figures

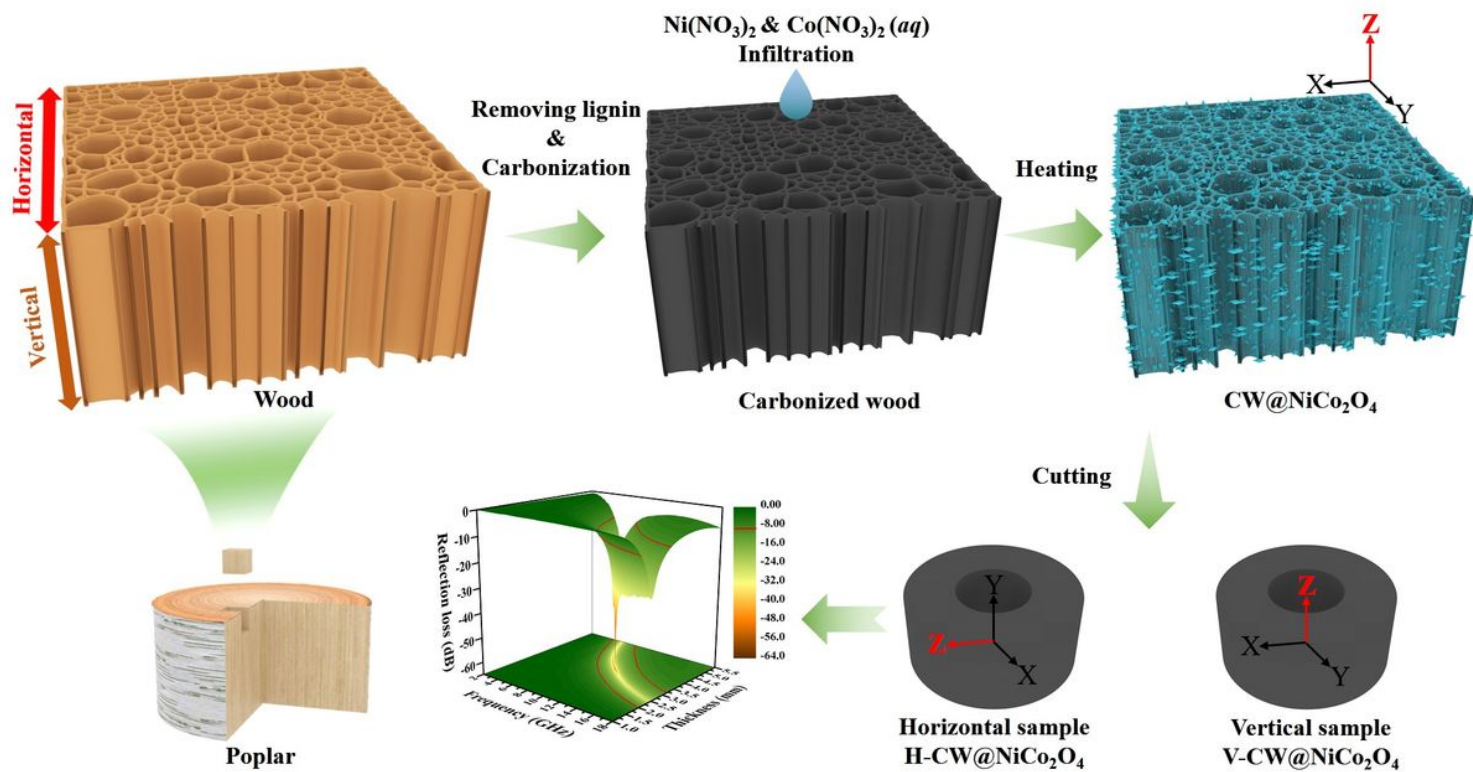


Figure 1

Fabrication process of CW@NiCo₂O₄ with ordered channels, and schematic illustration to obtain vertical and horizontal standard coaxial samples.

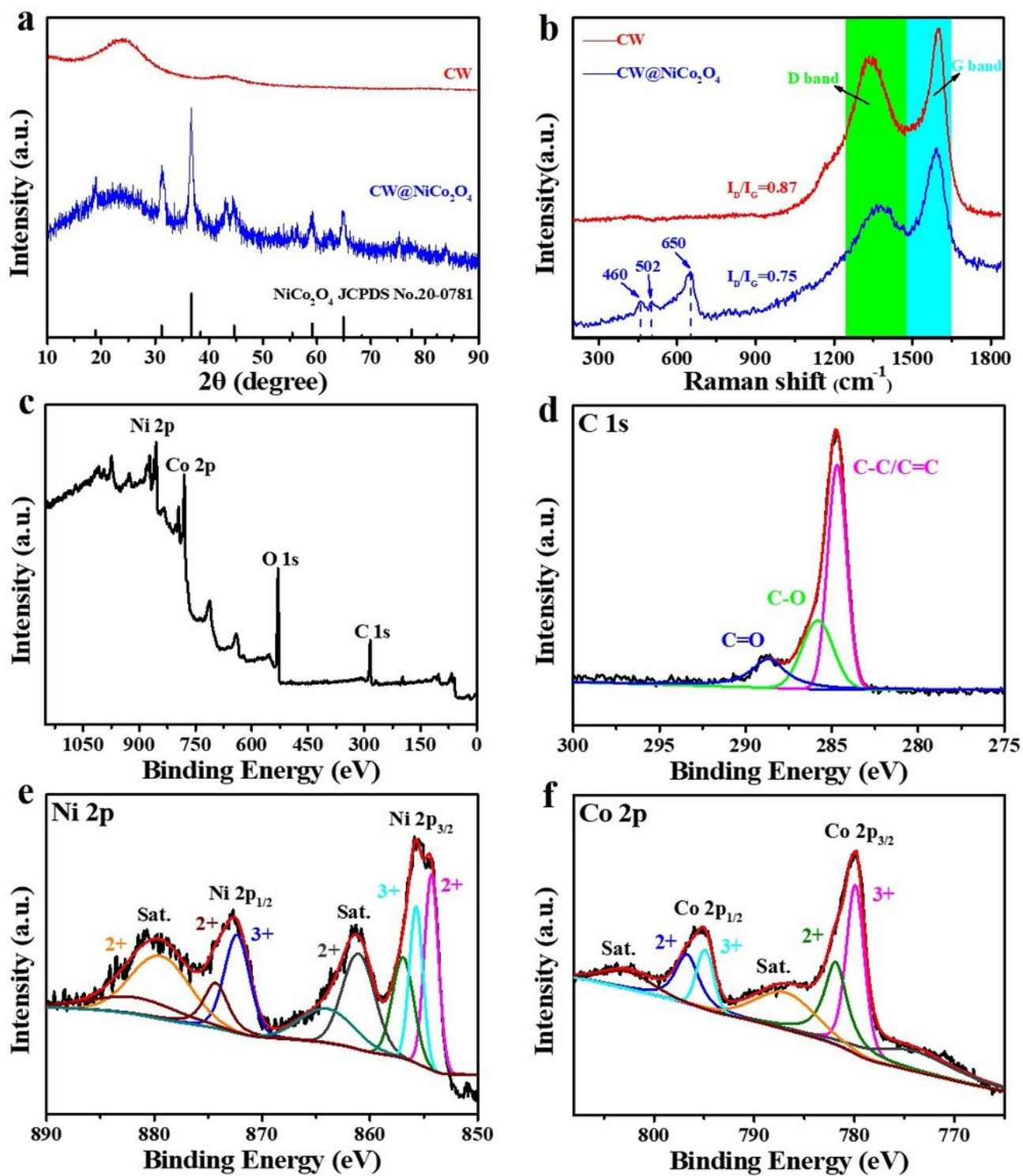


Figure 2

(a) XRD pattern of CW and CW@NiCo₂O₄; (b) Raman spectra of CW and CW@NiCo₂O₄; XPS spectra of CW@NiCo₂O₄: (c) wide span; (d) C 1s; (e) Ni 2p; (f) Co 2p.

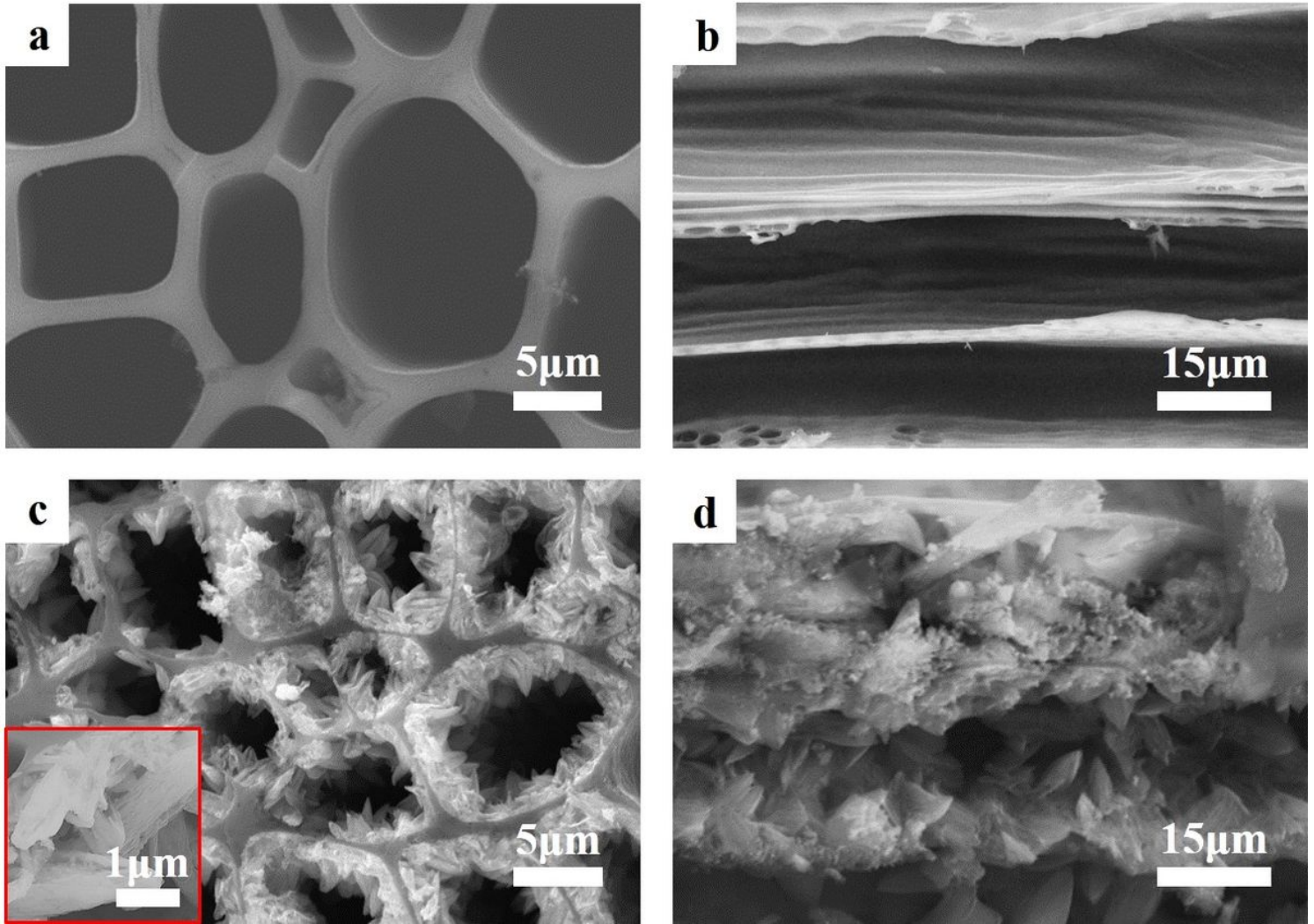


Figure 3

SEM images of (a) V-CW, (b) H-CW, (c) V-CW@NiCo₂O₄, (d) H-CW@NiCo₂O₄.

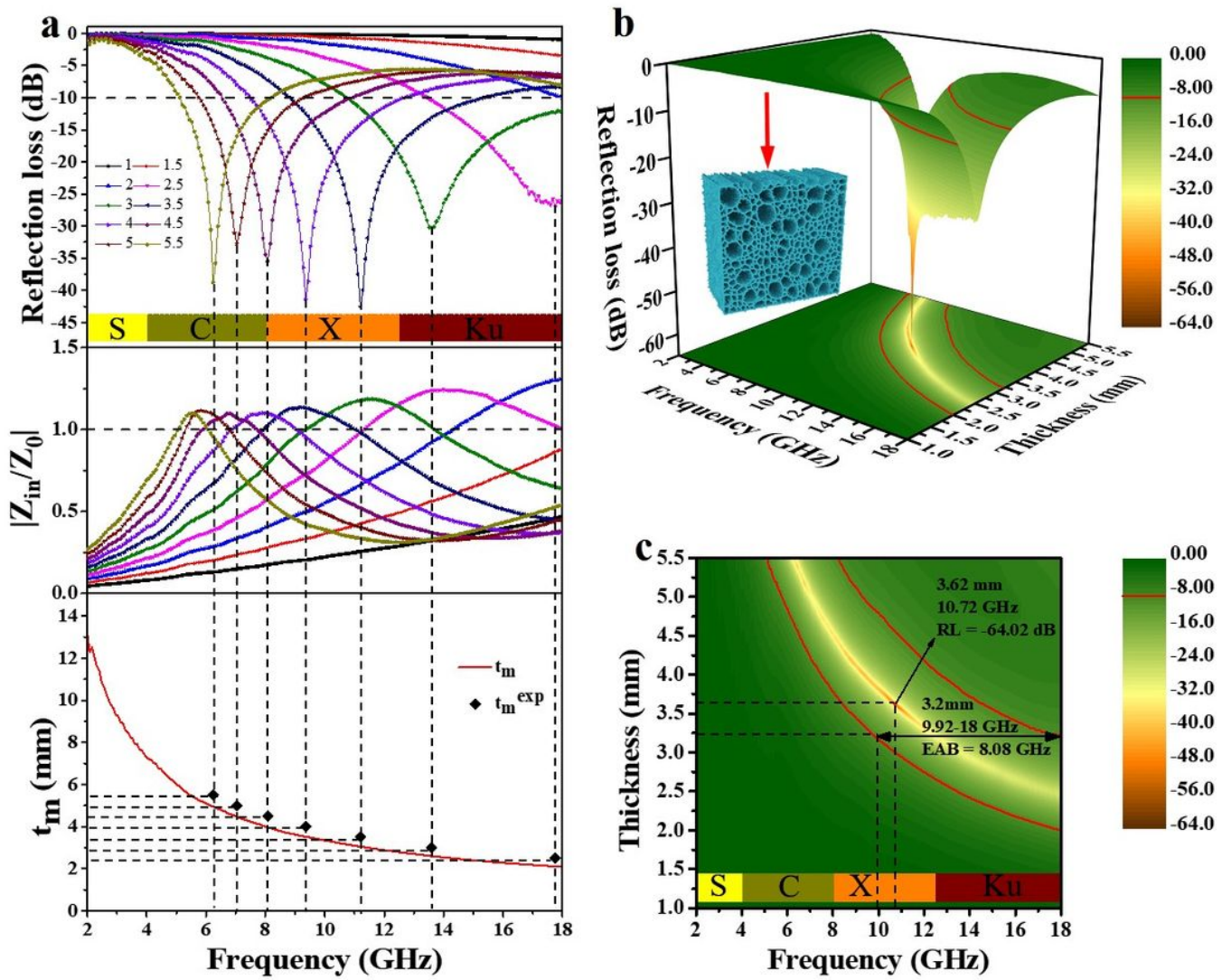


Figure 4

Please see the Manuscript PDF file for the complete figure caption.

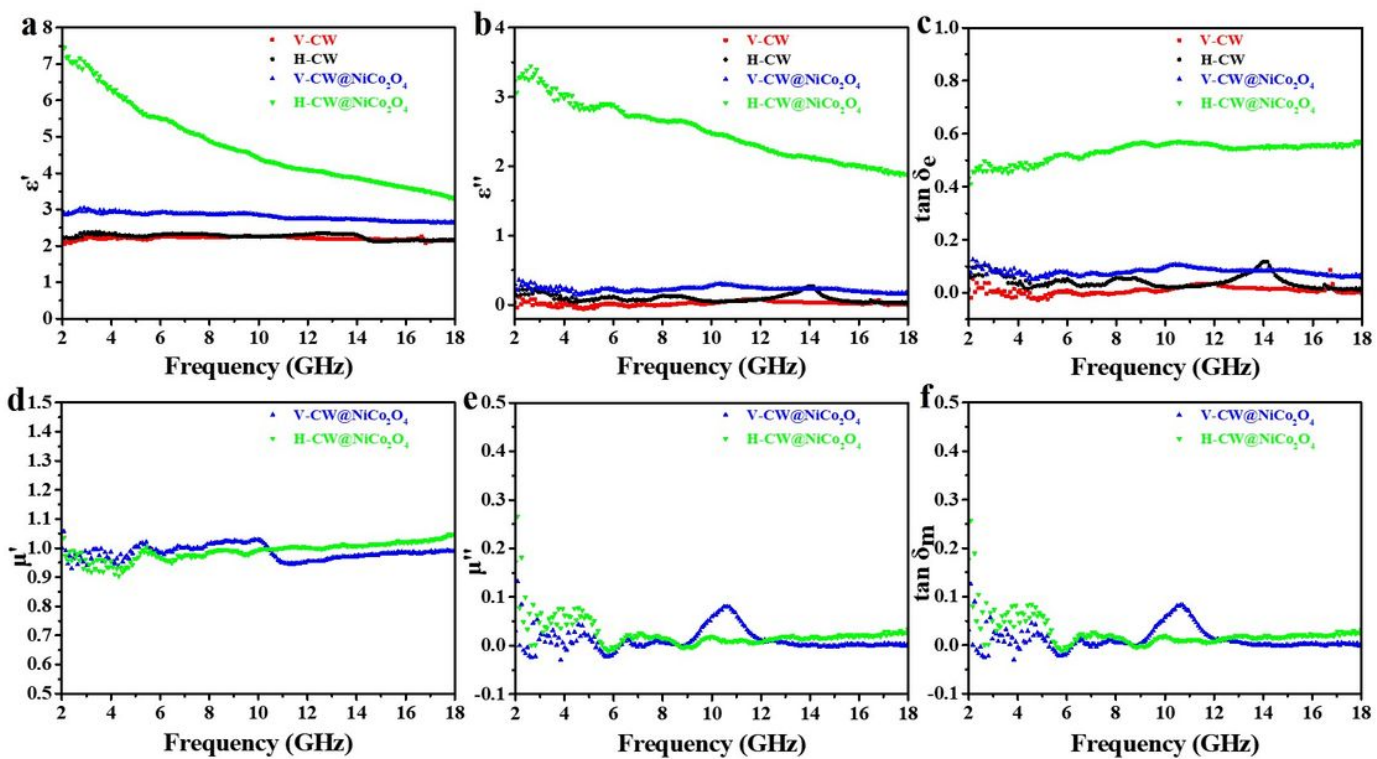


Figure 5

Please see the Manuscript PDF file for the complete figure caption.

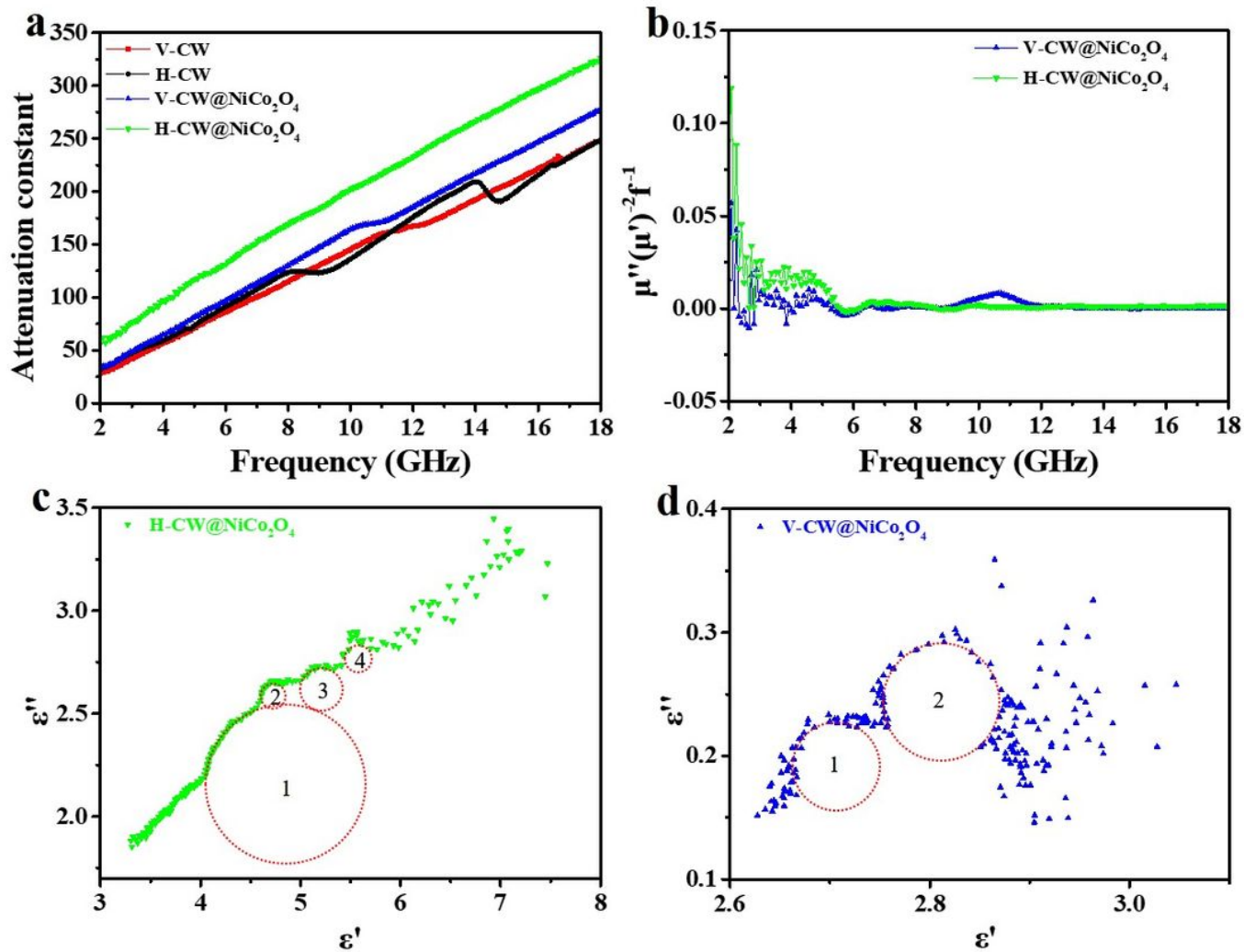


Figure 6

(a) Attenuation constant α of all samples, (b) C_0 values versus frequency of V-CW@NiCo₂O₄ and H-CW@NiCo₂O₄, Cole-Cole curves of (c) H-CW@NiCo₂O₄ and (d) V-CW@NiCo₂O₄.

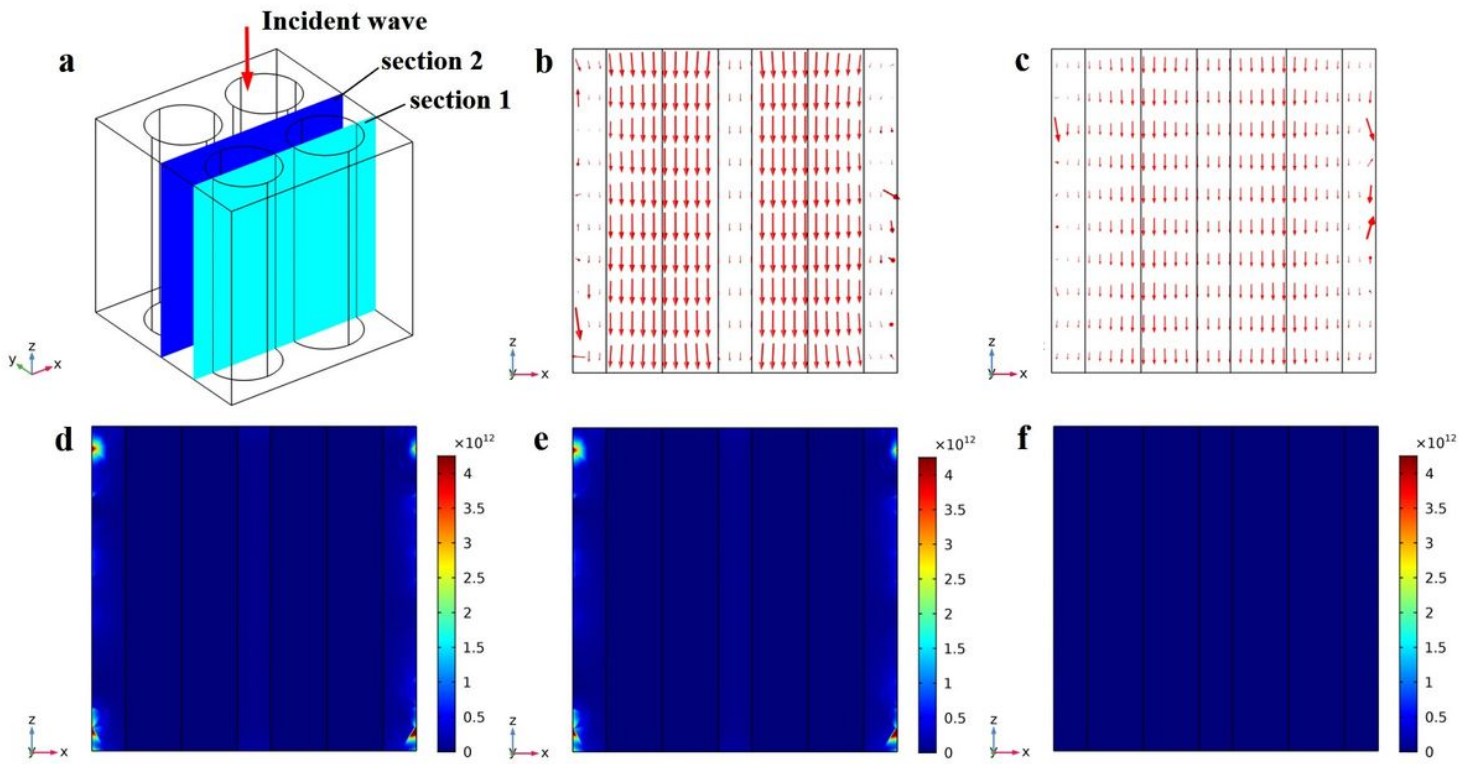


Figure 7

Please see the Manuscript PDF file for the complete figure caption.

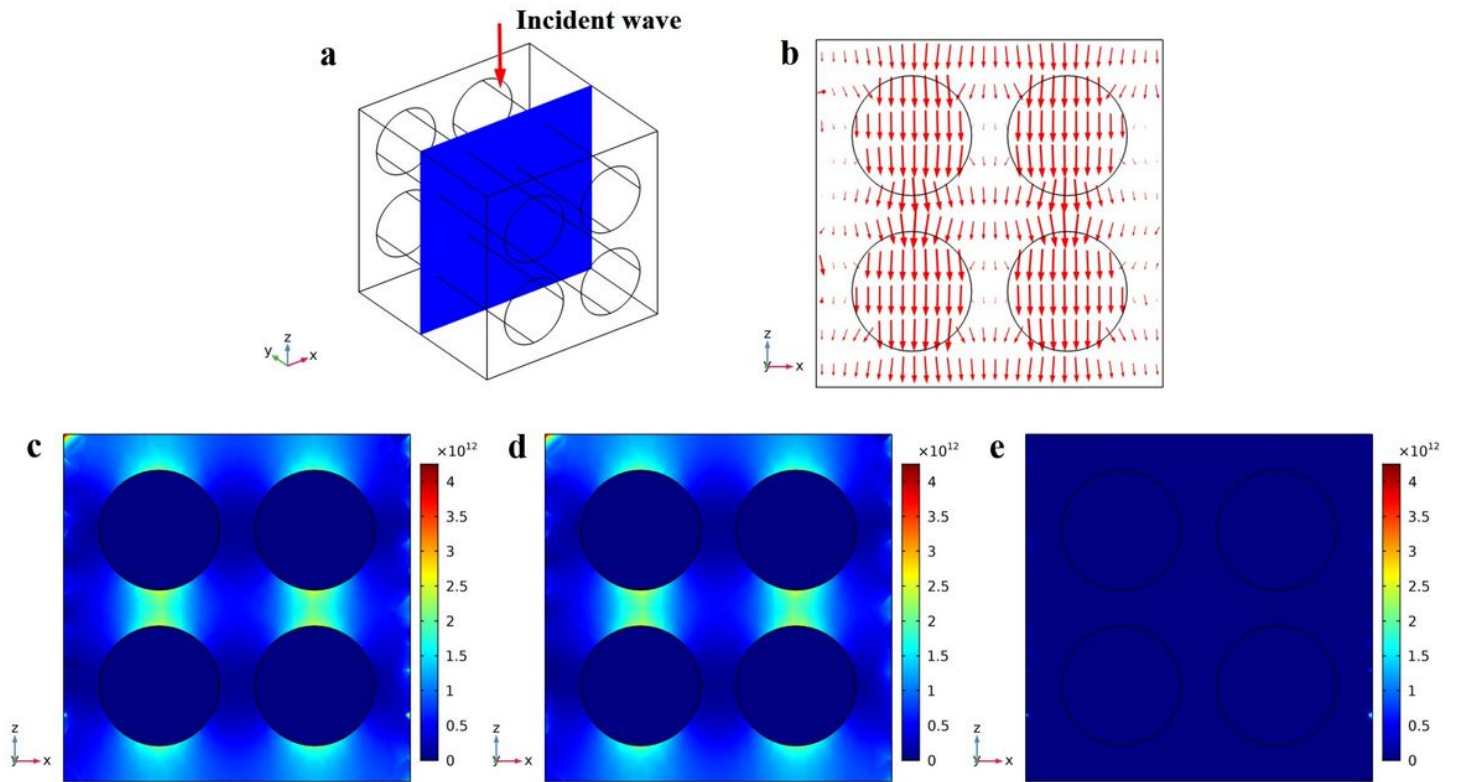


Figure 8

Please see the Manuscript PDF file for the complete figure caption.

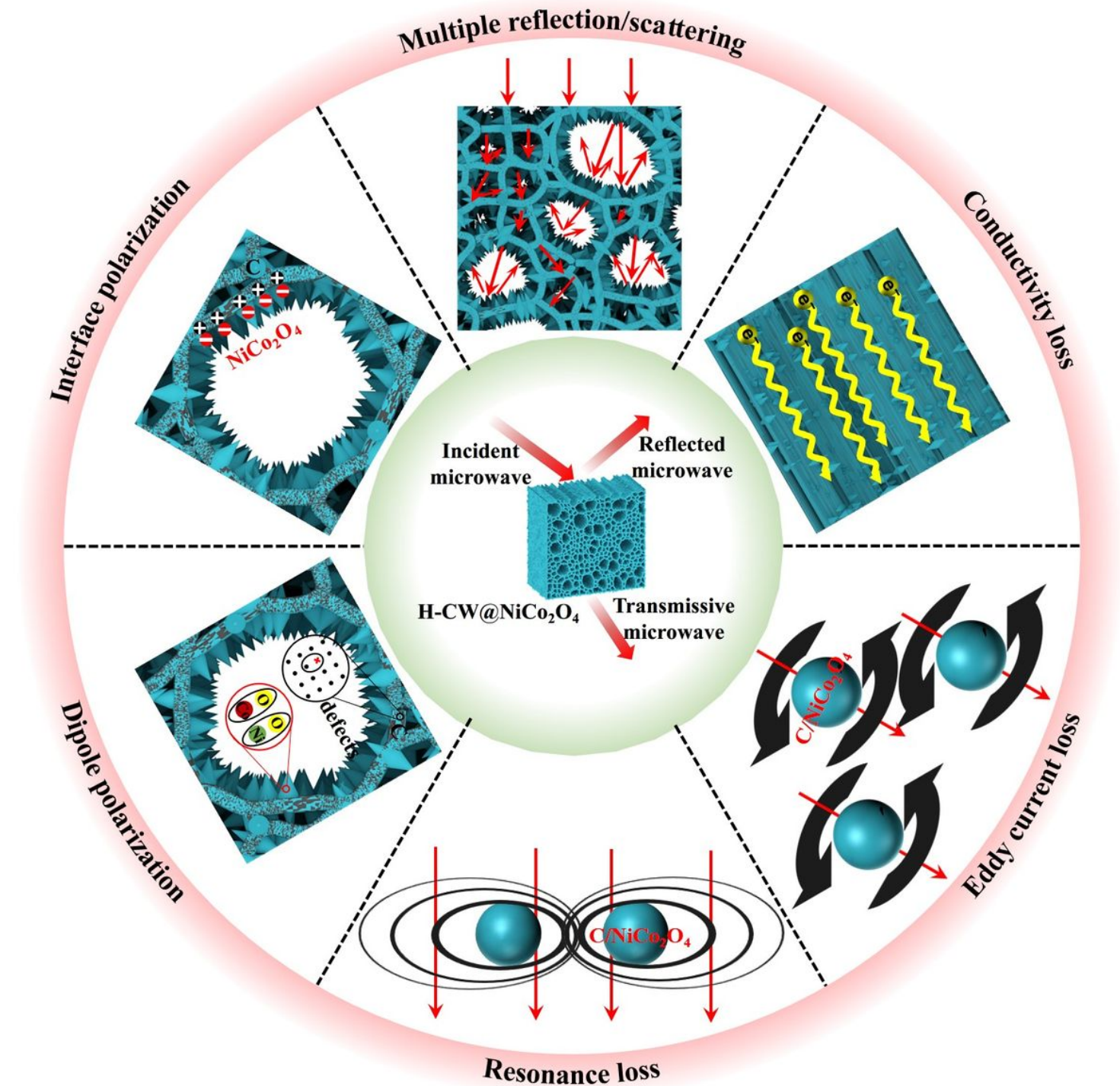


Figure 9

Schematic illustration for the EMW absorption of H-CW@NiCo₂O₄.

Supplementary Files

This is a list of supplementary files associated with this preprint. Click to download.

- [FigS1.jpg](#)
- [FigS2.jpg](#)
- [FigS3.jpg](#)
- [FigS4.jpg](#)
- [FigS5.jpg](#)
- [FigS6.jpg](#)
- [FigS7.jpg](#)